



Cite this: *RSC Adv.*, 2016, 6, 41687

Magnetic nanoparticle-supported ferrocenylphosphine: a reusable catalyst for hydroformylation of alkene and Mizoroki–Heck olefination†

M. Nasiruzzaman Shaikh,^{*a} Md. Abdul Aziz,^a Aasif Helal,^a Mohamed Bououdina,^b Zain H. Yamani^a and Tae-Jeong Kim^c

We present dopamine (dop) conjugated bis(diphenylphosphino)ferrocenylethylamine (BPPFA) functionalized magnetic nanoparticles (Fe_3O_4). A ferrocene ($\{\eta^5\text{-C}_5\text{H}_4\text{-PPh}_2\}\text{Fe}\{\eta^5\text{-C}_5\text{H}_3\text{-1-PPh}_2\text{-2-CH(Me)NH-CH}_2\text{-CH}_2\text{-4Ph-1,2-OH}\}$) ligand (dop-BPPF) has been prepared by reaction of (1-[1',2'-bis(diphenylphosphino)ferrocenyl]ethyl acetate) and dopamine hydrochloride to form dop-BPPF, which was characterized by NMR, IR, FTIR, EA and FAB-MS. This ligand was anchored on ultrasmall (6–8 nm) magnetic nanoparticles (MNP) to yield $\text{Fe}_3\text{O}_4\text{@dop-BPPF}$. The resulting ferrocenylphosphine on magnetic nanoparticles was characterized by SEM, EDS, XRD, TEM, TGA, and VSM. The magnetic nature of the materials was investigated. $\text{Fe}_3\text{O}_4\text{@dop-BPPF}$ exhibits very high catalytic activity for the Pd-catalyzed Mizoroki–Heck reaction and exceptionally high regioselectivity for the Rh-catalyzed hydroformylation reaction with branched aldehydes (up to > 99%). The potential of this $\text{Fe}_3\text{O}_4\text{@dop-BPPF}$ as a reusable catalyst has been studied for the Mizoroki–Heck reaction, and this catalyst was robustly active even after eleven consecutive cycles.

Received 11th February 2016
Accepted 18th April 2016

DOI: 10.1039/c6ra03859j

www.rsc.org/advances

Introduction

Carbon–carbon bond formation reactions mediated by various transition metals have emerged as increasingly important methodologies for the preparation of numerous organic building blocks, such as drugs^{1,2} pesticides,³ dye⁴ and natural products.^{5,6} Among the many frequently used C–C bond formation protocols, such as Stille,⁷ Heck,⁸ Suzuki,^{9,10} Kumada,¹¹ and Sonogashira,¹² Mizoroki–Heck¹³ for olefination and alkene hydroformylation¹⁴ to the corresponding aldehyde is important in synthetic organic and industrial chemistry. These reactions are often catalyzed by different phosphine-based homogeneous Pd metal complexes. For example, PPh_3 ,¹⁵ $\text{P}(o\text{-Tol})_3$ (ref. 16) and $\text{P}(\text{Mes})_3$ (ref. 17) are used as a monodentate ligands, and dippb (1,4-bis[(diisopropyl)phosphino]butane),¹⁸ dipp (1,4-bis[(diisopropyl)phosphino]propane)¹⁹ and dppe (1,1'-bis(diphenylphosphino)ferrocene)²⁰ are considered bidentate ligands. In a similar fashion, Co-, Rh- and

Ir-based metal complexes have been used for hydroformylation in the presence of *syn gas* and are excellent regioselective catalysts.^{21–23} However, the separation of the catalyst from the reaction mixture by chromatography, distillation and extraction is highly tedious, cumbersome and economically less viable. In addition, the valuable metal and ligands used in the process are not recoverable or reusable, which limits the scope of this process for cost-effective application.

In this context, the development of environmentally benign, reusable and efficient organocatalyst is the central goal in current research to contribute towards a 'greener' and safe environment. Moreover, the use of a readily available feed-stock, such as highly toxic carbon monoxide, to produce more expensive functionalized organic intermediates *via* hydroformylation is important. Therefore, extensive efforts have been focused on the development of alternatives to homogeneous catalysis to minimize separation costs and maximize product purity. Therefore, heterogeneous catalysis has become an alternative choice.^{24,25} The heterogenization of catalysts is based on the immobilization of ligands or metal complexes over solid supports, such as zeolites,²⁶ polymers,²⁷ silica²⁸ and cellulose.²⁹ For example, Koten *et al.* demonstrated the anchoring of chiral BINAP ligands on the surface of silica, which is highly stable, robust and easy to functionalize for the hydrogenation reaction.²⁸ However, the majority of the heterogenized catalysts exhibit lower reactivity compared to that of

^aCenter of Research Excellence in Nanotechnology (CENT), King Fahd University of Petroleum and Minerals (KFUPM), Dhahran-31261, Saudi Arabia. E-mail: mshaikh@kfupm.edu.sa

^bDepartment of Physics, College of Science, University of Bahrain, PO Box 32038, Kingdom of Bahrain

^cInstitute of Biomedical Engineering Research, Medical School, Kyungpook National University, Buk-gu, Daegu, South Korea 702-911

† Electronic supplementary information (ESI) available. See DOI: 10.1039/c6ra03859j

their homogeneous counterpart because the catalytic sites dip inside the solid support and become inaccessible to the substrate, decreasing the overall reactivity.^{30,31} Furthermore, solid catalyst separation processes, such as filtration, emulsification, and centrifugation, are complex, which affects the activity and reduces the potential reusability of conventional heterogeneous catalysts.^{32,33}

Recently, nanoparticles have become an area of interest for a wide range of applications in numerous fields. The use of nanoparticles in catalysis is advantageous because (1) nanosize particles can be considered equivalent to homogenous systems due to the reduction in active sites being negligible compared to that of homogeneous systems. In addition, (2) the highly exposed surface area of the active component of the catalysts provides additional proximity between the catalytic centers and the reactants, increasing the catalytic activity.^{30,34} For example, the chemical and physical properties (*i.e.*, shape, size and morphology) of superparamagnetic iron oxide nanoparticles (SPION) can easily be manipulated. The synthesis of SPIONS is relatively uncomplicated, and the particles are easily functionalized.³⁵ Furthermore, SPIONS have the potential to provide catalyst recyclability due to their insolubility in organic solvents and their distinct magnetic nature, rendering their separation from the heterogeneous reaction system virtually effortless. Recently, Wang *et al.* developed a heterocyclic carbene ligand-coated magnetic system and reported encouraging results for the coupling reaction.³⁶ However, the immobilization of the linker, which contains the terminal coordinating group, on SPION remains a challenge. In a majority of the reported cases, amine ligands³⁷ have been used because they stabilize the nanoparticles to prevent aggregation, which produces excellent results for the hydrogenation,³⁸ coupling³⁹ and oxidation⁴⁰ reactions. In this context, dopamine has become the most widely used linker⁴¹ because it affords higher stability to the nanoparticle surface and provides a suitable supporting arm for further functionalization. To achieve optimum balance between stability and catalytic activity, a suitable donor, such as diphenylphosphine, could be coordinated to the metal, and this group could be linked to dopamine to afford excellent catalytic materials. Therefore, we selected ferrocenyldiphosphine for use as this donor.

During the past few decades, ferrocene-based ligands have been widely studied due to their electron-rich aromatic structural motifs that undergo electrophilic aromatic substitution. In addition, their relatively low cost, thermal stability, high tolerance to moisture and oxygen and very unique chemical properties make these materials attractive. Despite the impressive progress in ferrocene-based homogeneous catalysis, the use of ferrocene in heterogeneous catalysis has remained largely unexplored. Therefore, ferrocenyldiphosphine with its unique stereochemical properties and various prospective coordination modes and superparamagnetic iron oxide nanoparticles were combined for use in regioselective catalytic reactions in a low-cost and environmentally friendly manner.

As a part of our continuing efforts,^{42–44} we report the synthesis of a new ferrocene-based ligand (**dop-BPPF**, $\{\eta^5\text{-C}_5\text{H}_4\text{-PPh}_2\}\text{Fe}\{\eta^5\text{-C}_5\text{H}_3\text{-1-PPh}_2\text{-2-CH(Me)NH-CH}_2\text{-CH}_2\text{-4C}_6\text{H}_3\text{-1,2-OH}\}$)

from BPPFA-OAc (1-[1',2-bis(diphenylphosphino)-ferrocenyl] ethyl acetate). This organic moiety was anchored on superparamagnetic iron oxide nanoparticles (SPION) *via* its phenolic 1,2-dihydroxide attached to dopamine. The $\text{Fe}_3\text{O}_4@$ **dop-BPPF**, $\text{Fe}_3\text{O}_4@$ **dop-BPPF-Rh** and $\text{Fe}_3\text{O}_4@$ **dop-BPPF-Pd** nanomaterials were characterized using various techniques, such as TEM, SEM-EDS, XRD, TGA, FTIR, and VSM. Their catalytic applications to the Pd-catalyzed Mizoroki–Heck and Rh-catalyzed regioselective hydroformylations of olefins were investigated.

Experimental

Materials and methods

All of the chemicals, which were purchased from Sigma-Aldrich, were used as received unless otherwise stated. An inert atmosphere and standard Schlenk techniques were used wherever needed. Standard procedures were followed for the dry and deoxygenated solvents. Deionized (DI) water was used throughout the experiments. The surface coating was carried out in a low-power bath sonicator (Cole-Parmer model 08892-21). The ^1H and ^{13}C NMR spectra were recorded on a JEOL JNM-LA 500 spectrometer with tetramethylsilane (TMS) as the internal standard. The ^{31}P NMR spectra were recorded on the same machine using a phosphorous probe and 85% H_3PO_4 as the internal reference. The FTIR spectra were obtained on a Nicolet 720 in the range of 400 to 4000 cm^{-1} using KBr. The thermogravimetric analysis (TGA) data were obtained on a Mettler-Toledo model TGA1 STAR^c System at a heating rate of 10 $^\circ\text{C min}^{-1}$ in a temperature range of 25–600 $^\circ\text{C}$ in an argon atmosphere. The X-ray diffraction data were collected on a Rigaku model Ultima-IV diffractometer using Cu-K α radiation.

The nanoparticles were imaged by field emission scanning electron microscopy (FESEM) on a LYRA 3 Dual Beam Tescan operated at 30 kV. The SEM samples were prepared from ethanolic suspensions on alumina stabs and coated with gold in an automatic gold coater (Quorum, Q150T E). For the elemental analysis and mapping, the energy dispersive X-ray spectra (EDS) were collected on a Lyra 3. The transmission electron microscope images were collected on a TEM (JEOL, JEM 2011) operated at 200 kV with a 4k \times 4k CCD camera (Ultra Scan 400SP, Gatan). The TEM samples were prepared by dropwise application of an ethanolic suspension onto a copper grid followed by drying at room temperature. The catalytic reactions were performed in a STEM Omni[®] 10-place reaction station and a Teflon-lined autoclave from HiTech, USA (model: M010SSG0010-E129A-00022-1D1101), which was equipped with a pressure gauge and mechanical stirrer. The magnetic susceptibilities were measured using a vibrating sample magnetometer (VSM, model PMC Micromag 3900) that was equipped with a 1 tesla magnet at room temperature. The products were identified using GCMS 2010 Plus from Shimadzu, Japan. The syntheses of *N,N*-dimethylferrocenyl ethyl amine (FA), *N,N*-dimethyl-1-[1',2-bis(diphenylphosphino)ferrocenyl] ethyl amine (BPPFA) and 1-[1',2-bis(diphenylphosphino)ferrocenyl]ethyl acetate (BPPFA-OAc) were performed according to previously reported procedures.^{45,46}

General procedure

Synthesis of $\{\eta^5\text{-C}_5\text{H}_4\text{-PPh}_2\}\text{Fe}\{\eta^5\text{-C}_5\text{H}_3\text{-1-PPh}_2\text{-2-CH(Me)NH-CH}_2\text{-CH}_2\text{-4Ph-1,2-OH}\}$ (dop-BPPF). To a solution of BPPFA-OAc (0.28 g, 0.43 mmol) in anhydrous methanol (10 mL), dopamine hydrochloride (0.19 g, 1.0 mmol) and freshly distilled triethylamine (1 mL) were added under an argon atmosphere. The mixture was stirred at 85 °C for 12 hours, and then, the solvent was removed under vacuum. The solid residue was dissolved in a minimal amount of methanol and transferred to a silica gel column for chromatographic separation. The desired orange band was eluted using a combination of ethyl acetate and methanol (9 : 1) to produce orange solids after removal of the solvents. Recrystallization from methanol/cyclohexane yielded 0.18 g of product (56%). ^{31}P NMR (202 MHz, in DMSO- d_6): δ -28.14 (s, PPh₂), -20.78 (s, PPh₂). ^1H NMR (DMSO- d_6): δ 1.30 (d, J = 6.7, 3H, CHCH₃), 1.78 (t, 2H, NCH₂CH₂), 2.29 (t, 2H, NCH₂CH₂), 3.55 (m, 3H, C₅H₃), 4.04–4.49 (m, 4H, C₅H₄), 6.20 (d, 1H, C₆H₃), 6.39 (s, 1H, C₆H₃), 6.60 (d, 1H, C₆H₃), 7.24–7.50 (m, 20H, PPh₂), 8.62 (s, 1H, OH), 8.74 (s, 1H, OH). ^{13}C NMR (DMSO- d_6): 19.03 (CHCH₃), 35.12 (NCH₂CH₂), 69.37 (NCH₂CH₂), 72.81 (CHCH₃), 115.29, 118.91, 128.20, 129.23, 132.11 (C₆H₃), 132.67, 132.82, 133.04, 134.43, 143.20, 144.81 (C₅H₃, C₅H₄ and PPh₂). FTIR in KBr (cm⁻¹): ν = 3426 (O-H), 3058 (arC-H), 2920 (Csp³-H) 1522 (arC-C). FAB-MS (m/z): calc. for C₄₄H₄₁FeNO₂P₂, 733.198 ([M]⁺); found, 733.196. Anal. calcd for C₄₄H₄₁FeNO₂P₂·CH₃OH: C, 70.59; H, 5.92; N, 1.83. Found: C, 70.67; H, 6.17; N, 2.01.

Synthesis of $\text{Fe}_3\text{O}_4@(\{\eta^5\text{-C}_5\text{H}_4\text{-PPh}_2\}\text{Fe}\{\eta^5\text{-C}_5\text{H}_3\text{-1-PPh}_2\text{-2-CH(Me)NH-CH}_2\text{-CH}_2\text{-4Ph-1,2-OH}\})$ ($\text{Fe}_3\text{O}_4@$ dop-BPPF). The magnetic nanoparticles (Fe₃O₄) were prepared according to a previously reported procedure.⁴² The magnetite nanoparticles (MNPs) were functionalized (Scheme 1) using a previously reported procedure^{35,42} that we modified as follows: to a suspension of magnetic nanoparticles (200 mg) in anhydrous chloroform, the ligand (200 mg) solution in dry methanol was added under an argon atmosphere. The mixture was sonicated in a bath sonicator for 6 hours. The surface functionalized magnetic nanoparticles were collected using a magnet after repeated washing with methanol followed by characterization. FTIR in KBr (cm⁻¹): ν = 3435 (O-H + N-H), 2938 (arC-H), 1428 (arC-C), 590 (Fe-O).

Synthesis of $\text{Fe}_3\text{O}_4@(\{\eta^5\text{-C}_5\text{H}_4\text{-PPh}_2\}\text{Fe}\{\eta^5\text{-C}_5\text{H}_3\text{-1-PPh}_2\text{-2-CH(Me)NH-CH}_2\text{-CH}_2\text{-4Ph-1,2-OH}\})\text{-M}$ ($\text{Fe}_3\text{O}_4@$ dop-BPPF-M). The magnetites nanoparticles (100 mg) in chloroform was sonicated for 1 hour. The solution of [Rh(NBD)Cl]₂ (0.015 mmol), slightly excess, in dichloromethane was added to the suspension and stirred for 4 hours under argon atmosphere. The materials was collected and washed with dichloromethane to remove unreacted metal precursor. The same procedure was followed with the $\text{Fe}_3\text{O}_4@$ dop-BPPF-Pd by replacing Rh with [Pd(C₃H₅)Cl]₂ (0.015 mmol).

Typical procedure for the catalytic hydroformylation reaction

This reaction was carried out in a functional fume hood fitted with good suction. The functionalized magnetic nanoparticles, $\text{Fe}_3\text{O}_4@$ dop-BPPF-Rh (50 mg), styrene (1.0 mmol, 0.12 mL) and freshly distilled THF (10 mL) were added to a Teflon-lined autoclave equipped with a pressure gauge and a mechanical stirrer under an argon atmosphere. Next, the inert atmosphere was replaced with a mild pressure release of CO/H₂ gas for three cycles. Then, the autoclave was pressurized with CO/H₂ (1 : 1) at 1000 psi, and the temperature was maintained at 45 °C. After completion of the reaction, the pressure was released, and the sample was passed through a short silica gel column followed by injection into a GC to determine the conversion and regioselectivity values.

Typical procedure for the catalytic Mizoriki–Heck reaction

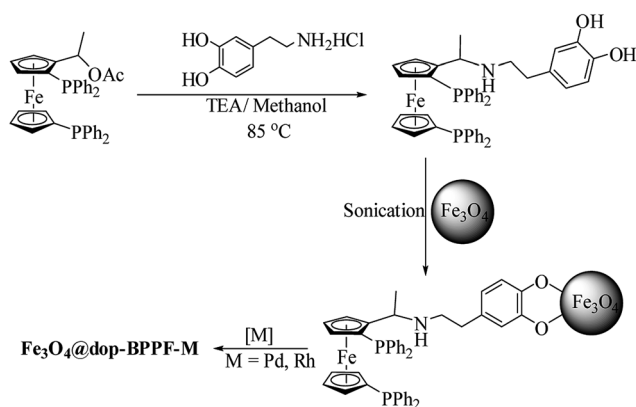
This reaction was performed in a parallel reactor 10 place reaction tube fitted with a magnetic stirrer and a Teflon stopper. To a suspension of functionalized magnetic nanoparticles, $\text{Fe}_3\text{O}_4@$ dop-BPPF-Pd (50 mg) in DMF : water (1 : 1) (10 mL), styrene (1.0 mmol, 0.12 mL) and potassium hydroxide (1.0 mmol, 56 mg) were added. The temperature was maintained at 90 °C. The progress of the reaction was monitored by GC, which was connected to a mass detector, and the product was extracted using ethyl acetate. The concentrated solution was passed through a short silica gel column and eluted with hexane : ethyl acetate (9 : 1).

Results and discussion

Synthesis

Magnetite nanoparticles 6–8 nm in size were prepared by reaction of divalent and trivalent iron in a 1 : 2 ratio in an alkaline medium at room temperature under an argon atmosphere with constant stirring (500 rpm). The pH of the solution was held constant with the periodic addition of conc. NH₄OH for 4 hours. A black precipitate was collected using a magnet and washed with DI water several times to remove any unreacted iron precursors.

Scheme 1 shows the preparation route for the formation of dopamine-functionalized ferrocenylphosphine. The synthetic route involved the preparation of *N,N*-dimethyl-1-ferrocenylethylamine (FA) followed by dilithiation and reaction with chlorodiphenylphosphine to afford BPPFA⁴⁷ (see the ESI†). The freshly prepared BPPFA was acetylated with the



Scheme 1 Synthesis of $\text{Fe}_3\text{O}_4@$ dop-BPPF-Pd and $\text{Fe}_3\text{O}_4@$ dop-BPPF-Rh.

replacement $-NMe_2$ functional group by reaction with acetic anhydride at 100 °C for 1 hour to yield BPPFA-OAc.⁴⁶

Dopamine hydrochloride was made soluble in anhydrous methanol in the presence of excess freshly distilled trimethylamine under an argon atmosphere with stirring. The solution consisting of BPPFA-OAc in methanol was added to the dopamine solution and refluxed for 12 hours at 85 °C to yield an orange color solid in good yield. Ferrocenylphosphine was linked with dopamine, which was used as an anchoring unit on the surface of the magnetic nanoparticles. Bidentate enediol ligands provide higher stability and tight binding to iron oxide by transforming under-coordinated Fe surface sites back to a bulk-like octahedral lattice structure for oxygen-coordinated magnetites,⁴⁸ and this behavior is further supported by the Langmuir isotherm, which indicated that the adsorption of dopamine *via* the 1,2-dihydroxyl functional group is more favorable than its desorption from the metal nanoparticles surface.⁴⁹ Therefore, we developed a system with a new organic ligand-coated magnetic nanostructure for use in catalytic organic transformation reactions.

Characterization

Structural confirmation of the new dopamine conjugated ferrocenylphosphine was based on spectroscopic and analytical analyses. Characteristic singlets appeared in the highly shielded (upfield) region (-20 and -28 ppm) in the ^{31}P NMR spectra and were assigned to the diphenylphosphine attached to the ferrocene ring (see the ESI[†]). The presence of ferrocenyl ring protons in the 3.5–4.5 ppm region, an axial methyl proton chemical shift (δ) at 1.30 ppm and three protons of the phenyl ring of

dopamine at 6.20, 6.39 and 6.60 ppm confirmed the formation of the desired compound, and this compound was further characterized by FAB-mass spectrometry and exhibited the characteristic molecular ion peak ($m/z = 733.196$) (see the ESI[†]).

Fig. 1a–d shows the TEM images of Fe_3O_4 (1a) $Fe_3O_4@$ dop-BPPF, $Fe_3O_4@$ dop-BPPF-Pd and $Fe_3O_4@$ dop-BPPF-Rh the results indicate that spherically shaped uniformly distributed nanosize particles were formed with an average diameter of 6–8 nm. The high-resolution TEM and selected area electron diffraction (SAED) images are shown in Fig. 1e and f respectively, and the inter planar distance was determined to be

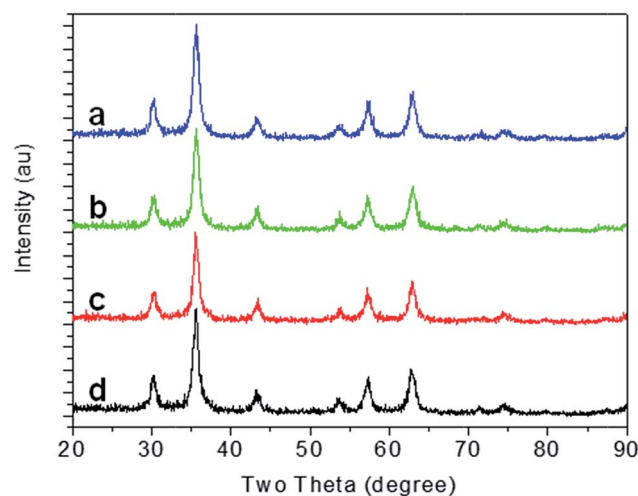


Fig. 2 XRD pattern of the (a) Fe_3O_4 and (b) $Fe_3O_4@$ dop-BPPF (c) $Fe_3O_4@$ dop-BPPF-Pd (d) $Fe_3O_4@$ dop-BPPF-Rh.

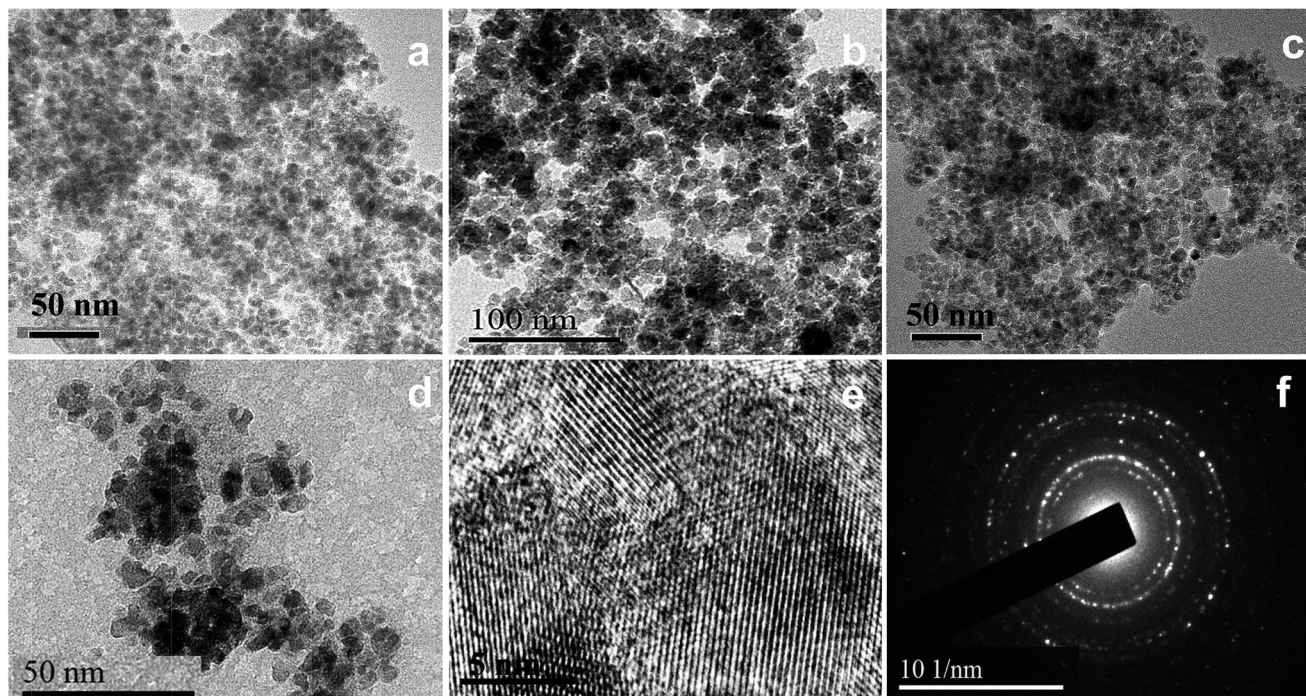


Fig. 1 TEM images of (a) Fe_3O_4 and (b) $Fe_3O_4@$ dop-BPPF (c) $Fe_3O_4@$ dop-BPPF-Pd (d) $Fe_3O_4@$ dop-BPPF-Rh (e) HRTEM image of $Fe_3O_4@$ dop-BPPF-Pd and (f) SAED of $Fe_3O_4@$ dop-BPPF-Pd.

consistent with the literature data.⁵⁰ The SAED data also exhibited higher order crystallinity, which was further confirmed by the X-ray diffraction (XRD) (Fig. 2) signature of the nanomaterial. The peaks located at 30.22°, 35.70°, 43.10°, 53.40°, 57.10° and 63.20° indicate the formation of a nanocrystalline cubic (*Fd3m*) spinel Fe_3O_4 nanostructure (JCPDS card no. 01-075-0449).⁵¹ Therefore, coating with **dop-BPPF** followed by addition with Pd/Rh did not alter the original crystal structure of the parent compound (Fe_3O_4). Qualitative and quantitative phase analyses were carried out using the Rietveld method. The refinement results and Rietveld figures (see the ESI†) also confirmed the formation of a single phase (goodness fit factor was close to 1). The calculated crystallite size was determined to be approximately 8.5 nm for all of the samples, which is in good agreement with the size obtained from TEM analysis. The calculated lattice parameter was approximately 8.36 Å, which is close to that of bulk magnetite. Elemental mapping (Fig. 3) analysis indicated the uniform anchoring of the ferrocenylphosphine ligands and its subsequent presence with the metal (*i.e.*, Rh and Pd) on the surface of the nanoparticles, and the existence of these elements were confirmed by the EDS results. The Fourier transform infrared (FTIR) spectroscopic data revealed a vibration red shift of Fe–O by 7 nm from 583 nm for the parent magnetite with a bare surface. The characteristic aromatic C–H stretching at 2938 cm^{-1} and aromatic C–C at 1428 cm^{-1} confirmed the presence of the ligand on the surface. The thermal stabilities of the ligand were investigated, and the stepwise weight loss profile was determined under an argon atmosphere in a temperature range of 25–600 °C (see the ESI†). The amount of weight loss was determined to be approximately 14%, which indicated that the amount of loading on the nanoparticle surface was 0.2 mmol of **dop-BPPF** per gram of magnetic nanoparticles. These data were further confirmed by the amount of phosphine determined from the EDS results.

The recorded magnetic data revealed the superparamagnetic nature of all of the samples (Fig. 4) at room temperature. Prior to coating, the magnetization of the bare surface of the magnetites (Fe_3O_4) was 67 emu g^{-1} , and the magnetization the surface-coated nanoparticles (Fe_3O_4 @**dop-BPPF**) was 58 emu g^{-1} . It is important to note that the coercivity (H_c) and remanence (M_r) are not affected by the surface functionalization and

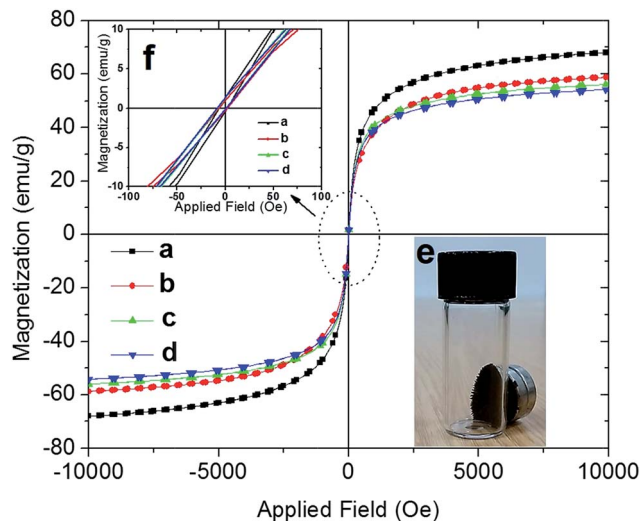


Fig. 4 Magnetic hysteresis loops of the (a) Fe_3O_4 (b) Fe_3O_4 @**dop-BPPF** (c) Fe_3O_4 @**dop-BPPF**-Pd (d) Fe_3O_4 @**dop-BPPF**-Rh at room temperature with 1 tesla magnet (e) Fe_3O_4 @**dop-BPPF**-Rh in presence of a magnet (f) The M_r and H_c in low M and H values. Inset for lower M and H values showing clearly M_r and H_c .

complexation processes. However, the saturation magnetization value slightly decreased due to coating and complexation (**dop-BPPF**, Pd and Rh). Therefore, these coating and existence of metal (Pd/Rh) did not substantially affect the bulk magnetization, which is very important for the separation process, and these data were further confirmed by the physical use of a magnet near to the vial containing the particles.

Catalysis

Hydroformylation reactions. The catalytic activity was evaluated using various substituted styrenes and *n*-alkenes at 45 °C with a mixture of carbon monoxide and hydrogen (1 : 1) under a pressure of 1000 psi. The results are shown in Table 1. The optimization of the conditions was performed using styrene as a model substrate. At 45 °C, 85% conversion of styrene to the corresponding aldehyde was achieved with a branched (B) to linear (L) ratio of 8 : 1 at 200 psi (entry #1). As the reaction temperature increased to 70 °C, the yield improved but the

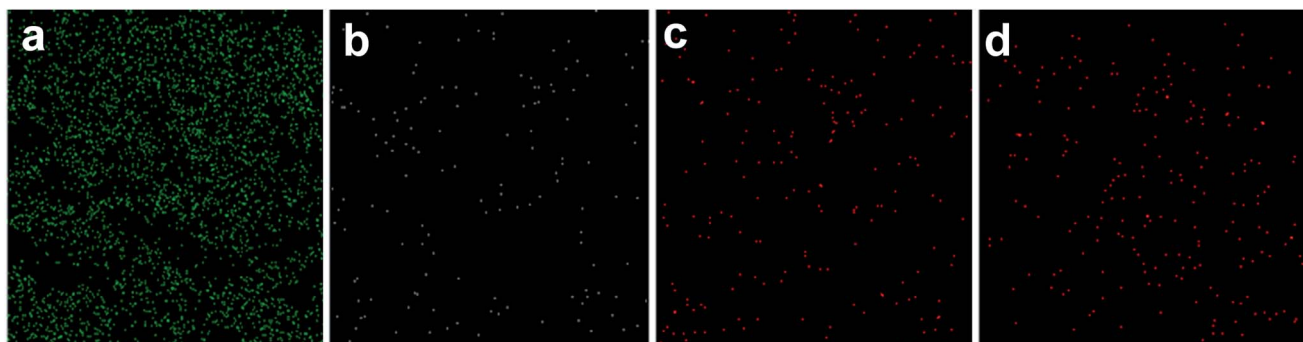


Fig. 3 Elemental mapping of (a) iron, (b) phosphorous (c) palladium and (d) rhodium of Fe_3O_4 @**dop-BPPF**.

Table 1 Hydroformylation^a of olefins using Fe₃O₄@dop-BPPF-Rh as catalysts

C=Cc1ccccc1
 $\xrightarrow[\text{CO:H}_2 (1:1)/ \text{Solvent}]{\text{Fe}_3\text{O}_4@\text{dop-BPPF}/[\text{Rh}]}$
CC(=O)c1ccccc1 + CCC(=O)c1ccccc1

 Branched (B) Linear (L)

Entry	Substrate	Time (h)	Solv.	Temp (°C)	Conv. ^c (%)	Branch (B) (%)	Linear (L) (%)	Ratio (B : L)
1 ^b	Styrene	9	THF	45	85	88.6	11.4	8 : 1
2 ^b	Styrene	10	THF	70	91	48.1	51.9	0.9 : 1
3	Styrene	8	THF	45	>99	94.5	5.5	17 : 1
4	Styrene	8	DCM	45	>99	96.4	3.6	28 : 1
5	Styrene	14	No solv.	45	86	85.4	14.6	6 : 1
6	4-Methylstyrene	14	THF	45	>99	93.4	6.6	14 : 1
7	4-Methylstyrene	14	DCM	45	>99	98.1	1.9	52 : 1
8	4-Vinylanisole	14	DCM	45	>99	97.2	2.8	35 : 1
9	4-Chlorostyrene	12	DCM	45	>99	98.6	1.4	70 : 1
10	3-Nitrostyrene	13	DCM	45	>99	99	1	99 : 1
11	2-Bromostyrene	13	DCM	45	>99	99	1	99 : 1
12	Vinylbenzoate	16	DCM	45	96	nd	nd	nd
13	1-Octene	16	DCM	45	85	—	100	0 : 100

^a 1 mmol of styrene in 10 mL anhydrous solvent under *syn gas* (CO : H₂ 1 : 1) pressure using 50 mg of Fe₃O₄@dop-BPPF-Rh and Rh-metal precursor.

^b Done at 200 psi. ^c Determined by GC and identified by GC-MS; nd: not determined.

regioselectivity was lost (entry #2). The solvent polarity plays an important role in the selectivity. Based on the results in Table 1, a more polar solvent negatively affected the selectivity. Among all of the tested solvents, dichloromethane was the most efficient solvent for this reaction. For example, a higher selectivity (B : L = 17 : 1) was obtained by employing a pressure of 1000 psi in THF at 45 °C. However, a substantial improvement was observed when the same reaction was performed in dichloromethane, and the regioselectivity increased to 28 : 1 from 17 : 1 (entries #3 and 4) and 52 : 1 from 14 : 1 (entries #6 and 7) for styrene and 4-methylstyrene, respectively. This excellent selectivity towards the branched aldehyde can be hypothesized that may be due to (1) the metal binding sites being far away from the metal nanoparticle surface, causing little interference with the Rh metal center. In addition, (2) the steric environment around the phosphine coordinated to the metal resulted in the predominant production of one isomer. We employed different types of electron-withdrawing and donating groups on the styrene substrate for the hydroformylation reaction. Although no noticeable change in the reactivity was observed, a profound effect was observed for the selectivity. The selectivity ratio for the branched to linear isomers of nitrostyrene and bromostyrene was 99 : 1 (entries #10 and 11).

We also investigated the hydroformylation of styrene under solvent-free conditions and achieved 86% conversion (entry #5) with 85% branched isomer. For *n*-alkene, the reactivity of the catalyst is slow, and the conversion of 1-octene (entry #14) reached to 85% but the opposite selectivity exhibited a maximum value (B : L = 0 : 100). This result is consistent with previously reported data.²⁵

The recyclability of the catalysts was investigated by employing the optimized reaction conditions. After the first round of catalysis, the nanocatalysts were sufficiently washed with dichloromethane to remove any unwanted materials and reused for the 2nd round of catalysis without the addition of more Rh metal precursor. A gradual loss in the catalytic activity was observed after the 4th run, which may be due to a higher pressure being employed in the reaction system, and the active catalyst was leached from the surface of the magnetic nanoparticles.

Table 2 Optimization of Mizoroki–Heck reaction between iodobenzene and styrene^a

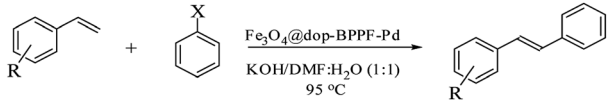
C=Cc1ccccc1 + Ic1ccccc1
 $\xrightarrow[\text{Base / Solvent}]{\text{Fe}_3\text{O}_4@\text{dop-BPPF-Pd}}$
C=Cc1ccc(cc1)-c2ccccc2

Entry	Base	Temp (°C)	Solvent	Conversion ^b (%)
1	KOH	60	DMF–H ₂ O (1 : 1)	50
2	KOH	95	DMF–H ₂ O (1 : 1)	99
3	K ₂ CO ₃	95	DMF–H ₂ O (1 : 1)	69
4	Et ₃ N	95	DMF–H ₂ O (1 : 1)	56
5	KOH	95	H ₂ O	67
6	KOH	95	Toluene	44
7	KOH	95	DMF	81

^a Conversion measured after 30 minutes of reaction and the conversions are based on iodobenzene. ^b Determined by GC and identified by GC-MS.

Mizoroki–Heck reactions. To optimize the reaction conditions of the Mizoroki–Heck reaction, styrene and iodobenzene were chosen as the model substrates to evaluate the catalytic activity. The results are shown in Table 2. The effect of the temperature was investigated. A higher temperature was determined to be effective, which was confirmed by the results in entries #1 and 2. At 95 °C, styrene was quantitatively converted to its corresponding product. However, at a lower temperature, the conversion was 50% (entry #1). In this reaction, the base plays a crucial role in the regeneration of Pd active species. Therefore, the K_2CO_3 , Et_3N and KOH bases were used in the $DMF : H_2O (1 : 1)$ mixture as a solvent, and the highest conversion was obtained using KOH (entry #2) compared to that using potassium carbonate or triethylamine (entries #3 and 4). The solvent effect was thoroughly investigated by employing a series of solvent systems, such as water, toluene, DMF and $DMF : water (1 : 1)$. The catalytic yield in pure water was only 67 (entry #5), which may be due to the organic substrate, which is highly insoluble in pure water, not being in sufficient contact with the metal reaction sites. However, the $DMF : water (1 : 1)$ mixture was a better solvent compared to that of pure DMF (entries #2 and 7).

Table 3 Mizoroki–Heck reaction^a between arylhalide and substituted styrene



Entry	Substrate (R)	Halide (X)	Time (min)	Conversion ^b
1	H	I	30	99
2	H	Br	30	78
			60	80
			120	96
			24 h	99
3	4-CH ₃	I	30	96
4	4-CH ₃	Br	30	87
			60	95
			120	98
5	4-OCH ₃	I	30	99
6	4-OCH ₃	Br	30	77
			60	94
			120	96
7	4-Cl	I	30	98
8	4-Cl	Br	30	35
			60	60
			120	66
			24 h	69
9	3-NO ₂	I	30	94
			60	97
10	3-NO ₂	Br	30	22
			60	27
			24 h	85
11	2-Br	I	30	96

^a Reactions were carried out at 95 °C in $DMF : H_2O (1 : 1)$ using KOH as base and $Fe_3O_4@dop-BPPF-Pd$; conversions are based on halobenzene.

^b Determined by GC and identified by GC-MS.

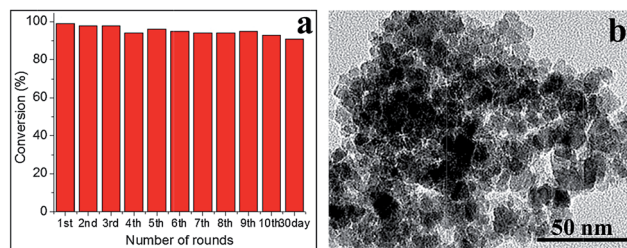


Fig. 5 (a) Re-usability studies of Mizoroki–Heck reaction of styrene and iodobenzene at 95 °C, in mixture of solvent $DMF : H_2O (1 : 1)$ using KOH as base (b) TEM image of the recovered catalyst.

Using the optimal reaction conditions, the coupling reaction was extended to a range of substituted styrene substrates to explore the scope of the newly developed catalytic system, and the results are summarized in Table 3. For example, as expected, bromobenzene was much less reactive with styrene than the corresponding iodobenzene (entries #1 and 2). However, prolonging the reaction time to 2–24 hours resulted in quantitative conversion. This result indicated the higher stability of the catalyst even after increasing the reaction time. The electron-withdrawing group in the *para* and *meta* of styrene (entries #7–10) decreased the reaction rate. For example, using 4-chlorostyrene (entry #7 and 8), the maximum conversion was 69% after 24 hour, and the same trend was observed for 3-nitrostyrene (entry #10), which yielded 85% of the coupling product.

The reusability of the nanocatalysts was investigating using the reaction of styrene and iodobenzene at 95 °C, and the results are shown in Fig. 5 as a bar diagram. After completion of the coupling reaction, the catalyst was collected by placing an external magnet at the bottom of the reaction vessel, and the solution was decanted for work up and GC measurements. The collected nanomaterials were repeatedly washed with ethyl acetate and water prior to use in the next round of catalysis. The catalyst exhibited a consistent activity up to the 10th consecutive cycle after the reaction time was increased to 12 hours. The TEM image (Fig. 5b) was obtained for the catalyst recovered after 10th cycle and no significant change was observed. Intrigued by its robustness, the collected catalysts from the 10th cycles were placed in the same coupling reaction for 30 days, and surprisingly, the observed loss of activity remained almost the same.

Conclusion

In summary, we have successfully developed ferrocenylphosphine ligand-coated magnetic nanomaterials for the hydroformylation and Mizoroki–Heck reactions. The use of the nanocatalyst in regioselective reactions of vinyl arenes and *n*-alkene resulted in very high branched isomer yields with excellent reactivity. The reaction was straightforward. In addition, no hydrogenated product was observed in the Rh-catalyzed hydroformylation, and no biphenyl product was observed in the Pd-catalyzed Mizoroki–Heck reaction. This system can be employed as a green catalyst in the hydroformylation reaction

without the use of any organic solvents. This material is highly robust, thermally stable and reusable for many consecutive cycles without the addition of more precious metals. The reusability may only be limited under high pressures (1000 psi or more) in the rhodium-catalyzed reaction. We believe that our simple synthetic strategy will open up a new area related to the attachment of functionalized ferrocene to metal oxide nanoparticle surfaces for various regio- and heterogeneous catalytic applications. The mechanism of action of the unusually high selectivity and its asymmetric version (*i.e.*, enantioselective hydrogenation, allylic alkylation, Michael addition and cyclopropanation) are currently under process in our lab.

Acknowledgements

MNS gratefully acknowledges the National Plan for Science, Technology and Innovation (MAARIFAH)-King Abdulaziz City for Science and Technology through the Science and Technology Unit at King Fahd University of Petroleum and Minerals (KFUPM), the Kingdom of Saudi Arabia, award number 15-NAN4650-04.

References

- O. Baudoin, M. Cesario, D. Guénard and F. Guéritte, *J. Org. Chem.*, 2002, **67**, 1199.
- M. A. Gauthier and H.-A. Klok, *Chem. Commun.*, 2008, 2591.
- D.-W. Ryu, D. N. Primer, J. C. Tellis and G. A. Molander, *Chem.-Eur. J.*, 2016, **22**, 120.
- A. Brennfuhrer, H. Neumann and M. Beller, *Angew. Chem., Int. Ed.*, 2009, **48**, 4114.
- T. Rybak and D. G. Hall, *Org. Lett.*, 2015, **17**, 4156.
- R. Liu, M. Zhang, T. P. Wyche, G. N. Winston-McPherson, T. S. Bugni and W. Tang, *Angew. Chem., Int. Ed.*, 2012, **51**, 7503.
- J. K. Stille, *Angew. Chem., Int. Ed.*, 1986, **25**, 508–524.
- R. F. Heck, *Acc. Chem. Res.*, 1979, **12**, 146.
- N. Miyaura and A. Suzuki, *Chem. Rev.*, 1995, **95**, 2457.
- A. Suzuki, *Chem. Commun.*, 2005, 4759.
- K. Tamao, K. Sumitani and M. Kumada, *J. Am. Chem. Soc.*, 1972, **94**, 4374.
- T. W. Lyons and M. S. Sanford, *Chem. Rev.*, 2010, **110**, 1147.
- N. T. S. Phan, M. V. D. Sluys and C. W. Jones, *Adv. Synth. Catal.*, 2006, **348**, 609.
- F. Ungvary, *Coord. Chem. Rev.*, 2007, **251**, 2087.
- H. A. Dieck and R. F. Heck, *J. Am. Chem. Soc.*, 1974, **96**, 1133.
- R. F. Heck, *Pure Appl. Chem.*, 1978, **50**, 691.
- W. A. Herrmann, C. Brobmer, K. Ofele, M. Beller and H. Fischer, *J. Mol. Catal. A: Chem.*, 1995, **103**, 133.
- Y. Bendavid, M. Portnoy, M. Gozin and D. Milstein, *Organometallics*, 1992, **11**, 1995.
- M. Portnoy, Y. Bendavid and D. Milstein, *Organometallics*, 1993, **12**, 4734.
- T. Jia, P. Cao, B. Wang, Y. Lou, X. Yin, M. Wang and J. Liao, *J. Am. Chem. Soc.*, 2015, **137**, 13760.
- C. Godard, S. B. Duckett, S. Polas, R. Tooze and A. C. Whitwood, *Dalton Trans.*, 2009, **14**, 2496.
- C. Kubis, M. Sawall, A. Block, K. Neymeyr, R. Ludwig, A. Bçrner and D. Selent, *Chem.-Eur. J.*, 2014, **20**, 11921.
- I. Piras, R. Jennerjahn, R. Jackstell, A. Spannenberg, R. Franke and M. Beller, *Angew. Chem., Int. Ed.*, 2011, **50**, 280.
- P. Wang, X. Liu, J. Yang, Y. Yang, L. Zhang, Q. Yang and C. Li, *J. Mater. Chem.*, 2009, **19**, 8009.
- R. Abu-Reziq, H. Alper, D. Wang and M. L. Post, *J. Am. Chem. Soc.*, 2006, **128**, 5279.
- (a) H. Zhang, Y. Zou, Y.-M. Wang, Y. Shen and X. Zheng, *Chem.-Eur. J.*, 2014, **20**, 7830; (b) Z.-M. Li, Y. Zhou, D.-J. Tao, W. Huang, X.-S. Chen and Z. Yang, *RSC Adv.*, 2014, **4**, 12160.
- (a) H. Zhang, W. Yang and J. Deng, *Polymer*, 2015, **80**, 115; (b) L. Li, C. Zhou, H. Zhao and R. Wang, *Nano Res.*, 2015, **83**, 709.
- (a) Y. Maegawa and S. Inagaki, *Dalton Trans.*, 2015, **44**, 13007; (b) J. M. Bolivar, S. Schelch, T. Mayr and B. Nidetzky, *ACS Catal.*, 2015, **5**, 5984; (c) M. Rimoldi, D. Fodor, J. A. van Bokhoven and A. Mezzetti, *Catal. Sci. Technol.*, 2015, **5**, 4575; (d) A. R. McDonald, C. Müller, D. Vogt, G. P. M. van Klink and G. van Koten, *Green Chem.*, 2008, **10**, 424.
- S. Zhou, M. Johnson and J. G. C. Veinot, *Chem. Commun.*, 2010, **46**, 2411.
- V. Polshettiwar, B. Baruwati and R. S. Varma, *Chem. Commun.*, 2009, 1837.
- R. S. Varma, *Pure Appl. Chem.*, 2013, **85**, 1703.
- S. Vellalath, I. Coric and B. List, *Angew. Chem., Int. Ed.*, 2010, **49**, 9749.
- M. Gemmeren, F. Lay and B. List, *Aldrichimica Acta*, 2014, **47**, 3.
- V. Polshettiwar and R. S. Varma, *Green Chem.*, 2010, **12**, 743.
- C. O. Dalaigh, S. A. Corr, Y. Gunko and S. J. Connon, *Angew. Chem., Int. Ed.*, 2007, **46**, 4329.
- Z. Wang, Y. Yu, Y. X. Zhang, S. Z. Li, H. Qian and Z. Y. Lin, *Green Chem.*, 2015, **17**, 413.
- F. Zhang, J. Jin, X. Zhong, S. Li, J. Niu, R. Li and J. Ma, *Green Chem.*, 2011, **13**, 1238.
- A. J. Amali and R. K. Rana, *Green Chem.*, 2009, **11**, 1781.
- B. Baruwati, D. Guin and S. V. Manorama, *Org. Lett.*, 2007, **9**, 5377.
- V. Polshettiwar and R. S. Varma, *Org. Biomol. Chem.*, 2009, **7**, 37.
- C. Duanmu, L. Wu, J. Gu, X. Xu, L. Feng and X. Gu, *Catal. Commun.*, 2014, **48**, 45.
- M. N. Shaikh, M. Bououdina, A. A. Jimoh, M. A. Aziz, A. Helal, A. S. Hakeem, Z. H. Yamani and T.-J. Kim, *New J. Chem.*, 2015, **39**, 7293.
- M. N. Shaikh, V. D. M. Hoang and T.-J. Kim, *Bull. Korean Chem. Soc.*, 2009, **30**, 3075.
- H.-K. Kim, J.-A. Park, K. M. Kim, M. N. Shaikh, D.-S. Kang, J. Lee, Y. Chang and T.-J. Kim, *Chem. Commun.*, 2010, **46**, 8442.
- G.-H. Hwang, E.-S. Ryu, D.-K. Park, S. C. Shim, C. S. Cho, T.-J. Kim, J. H. Jeong and M. Cheong, *Organometallics*, 2001, **20**, 5784.

- 46 T. Hayashi, T. Mise, M. Fukushima, M. Kagotani, N. Nagashima, Y. Hamada, A. Matsumoto, S. Kawakami and M. Konishi, *Bull. Chem. Soc. Jpn.*, 1980, **53**, 1138.
- 47 T. Hayashi, K. Yamamoto and M. Kumada, *Tetrahedron Lett.*, 1974, 4405.
- 48 G. W. Gokel and I. K. Ugi, *J. Chem. Educ.*, 1972, **49**, 294.
- 49 L. X. Chen, T. Liu, M. C. Thurnauer, R. Csencsits and T. Rajh, *J. Phys. Chem. B*, 2002, **106**, 8539.
- 50 T. Rajh, L. X. Chen, K. Lukas, T. Liu, M. C. Thurnauer and D. M. Tiede, *J. Phys. Chem. B*, 2002, **106**, 10543.
- 51 N. Pinna, S. Grancharov, P. Beato, P. Bonville, M. Antonietti and M. Niederberger, *Chem. Mater.*, 2005, **17**, 3044.